Numerical Analysis of Thermocapillary and Evaporating Flows at Low Bond Number

By

H. L. CHEN* , K. OSHIMA** and M. HINADA**

(February 10, 1989)

Summary: A numerical method using boundary-fitted coordinate system has been developed to analyze two-dimensional viscous flows with curvilinear surface at low Bond number. Evaporating liquid flows accompanied by thermocapillary convection, which model flows inside micro-heat pipes or those under microgravity environment, have been numerically analyzed. The effects of the thermocapillary force and the evaporation resistance on flow fields, the temperature distribution along the meniscus and the heat transfer rate have been numerically predicted.

NOMENCLATURE

Bo : Bond number
Bi : Biot number
Bic : Biot number to convection heat transfer
Bie : Biot number to evaporation heat transfer
D : width of the groove
g : the gravity acceleration
h : heat transfer coefficient
K : thermal conductivity
k : thermal diffusivity
L : latent heat
Ma : Marangoni number
P : pressure
Pr : Prandtl number
R : nondimensional evaporation resistance
r : evaporation resistance
Ra : Rayleigh number
T : Temperature
t : time
U : x component of the velocity vector
V : y component of the velocity vector
V : velocity vector
x, y : space variables in the Cartesian coordinate system
Δ : finite difference
ξ, η : space variables in the general coordinate system
κ : curvature of the meniscus
μ : dynamic viscousity
ν : kinematic viscosity
ρ : density
σ : surface tension coefficient
ψ : stream-function
ω : vorticity

Subscripts
i : node number in ξ direction
j : node number in η direction
t : time derivative
x : x direction derivative
y : y direction derivative
ξ : ξ direction derivative
η : η direction derivative
n : normal direction
τ : tangential direction

Superscripts
m : iterative step
n : time step

* Department of Aeronautical Engineering, Tokyo University.
** The Institute of Space and Astronautical Science.

1. Introduction

Surface-tension-driven phenomena are observed in a variety of flow problems related to two-phase systems [5]. These phenomena have been extensively investigated for many years. With recent progress of space technology, interests concerning the fluid problems in the space environment have greatly increased and it has been recognized that the surface tension effect is dominant in such environment [6, 7]. However, fundamental behavior of fluids in low-gravity environment is still unknown. Study of problems related to the surface tension became one of the most motivating topics in fluid mechanics.

In this study, we consider fluid motion induced by the surface tension, which is not a constant but varies according to the temperature. Inhomogeneous temperature distribution along the phase-boundary causes an inhomogeneous surface tension along the surface, then a flow is induced by tangential gradients of the surface tension. This is commonly called the thermocapillary flow.

Several theoretical and numerical investigations concerning to thermocapillary convection and to its flow stability have been carried out [2, 7, 9, 11] and understanding of this kind of fluid motion has been expanded beyond a certain extent. In such studies, the phase-boundary was usually assumed to be plane. However, it is well-known that, in the capillary-dominant motion, the phase-boundary surface is no longer flat. Analysis taking into account the curved phase-boundary surfaces are important.

On the other hand, evaporation from the meniscus is influenced by the capillary behavior of the liquid. The fluid temperature is higher in the neighborhood of the contact line than at far from it due to heating from the solid wall. Therefore, this temperature difference causes thermocapillary flow along the meniscus. This thermocapillary flow directly affects to evaporation and heat transfer. These effects have not been clarified yet.

In the study, a two-dimensional thermocapillary flow model including evaporation effect is proposed. The phase-boundary surface is assumed to be curved and it is determined as a function of the Bond number and the wall-liquid contact angle. The fluid is incompressible and viscous. This model is applicable to the fundamental flow behavior taking place inside micro-heat pipes or under low-gravity environment. Based on this model, a numerical scheme is developed to analyze the thermocapillary and evaporating flow problems. Finite difference method using the generalized coordinate system and the grid generation was applied to this curved boundary problem. In the following sections, the flow model, the numerical method and the computational results will be described in detail.

2. Physical and Mathematical Model

2.1 Physical model

A two-dimensional thermocapillary and evaporating flow model is schematically shown in Fig. 1. Liquid partly fills a two-dimensional groove. Fluid flow is considered to be steady, viscous, incompressible and laminar. Due to the assumption of capillary-dominant flow, the Bond number is low and the phase boundary between the liquid and the vapor is curvilinear. The contact angle α is assumed to be constant. Thermocapillary force and evaporation resistance act on the phase boundary. Gravity acceleration is in the downward direction. Liquid is heated from the heated wall which has an isothermal temperature T_1. Vapor is assumed to be inert, that is, it has a uniform, lower temperature T_0 than T_1 and no vapor motion takes place. This assumption of the inert vapor may not destroy our main purpose of this analysis, and such well simplified problem can be solved rather easily.

2.2 Mathematical model

Force balance among the pressure, the surface tension and the viscous stress must be fulfilled at the phase boundary. Because the effect of the fluid motion and the viscosity on the shape of the meniscus is not large [*12*], the meniscus is assumed to be same as the static meniscus;

$$\left.\begin{aligned} P/\rho g + y_0(x) &= H \\ P_v - P &= \kappa\sigma \\ \kappa &= \frac{d^2y_0/dx^2}{[1+(dy_0/dx)^2]^{3/2}} \end{aligned}\right\} \quad (1)$$

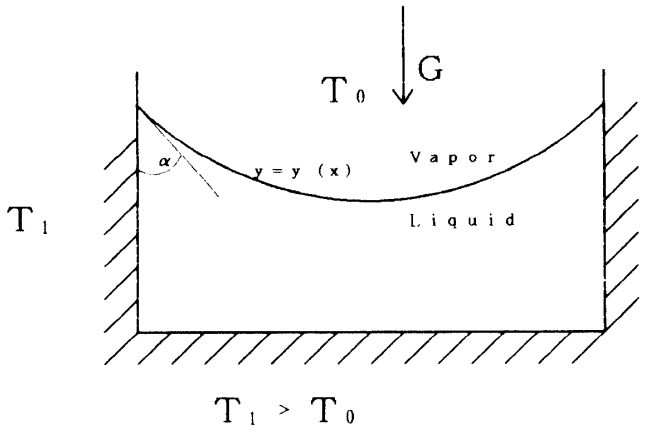

Fig. 1. Schematics of thermocapillary and evaporating flows.

Where P is the pressure, $y_0(x)$ is the meniscus line, H is a constant, P_v is the vapor pressure, σ is the surface tension coefficient and κ is the curvature of the meniscus line. Eq. (1) is nondimensionalized in the following form

$$\frac{d^2y_0/dx^2}{[1+(dy_0/dx)^2]^{3/2}}-Boy_0 = H \tag{2}$$

where $Bo=\rho gD^2/\sigma$, D is the width of the groove. The meniscus line is to be determined from Eq. (2).

Basic Equations expressing the conservation of mass, momentum and energy of liquid flow are, respectively,

$$\frac{\partial U}{\partial x}+\frac{\partial V}{\partial y} = 0 \tag{3}$$

$$\frac{\partial \mathbf{V}}{\partial t}+ (\mathbf{V}\cdot\nabla)\mathbf{V} = \nabla^2\mathbf{V}+R_aT\vec{g} \tag{4}$$

$$\frac{\partial T}{\partial t}+ (\mathbf{V}\cdot\nabla)\mathbf{V} = \frac{1}{Pr}\nabla^2T \tag{5}$$

$$Ra = \frac{D^3g\,\beta(T_1-T_0)}{\nu k}, \quad Pr=\frac{\nu}{k}$$

where Ra is the Rayleigh number and Pr is the Prandtl number. The Boussinesq approximation has been applied.

Non-slip and isothermal conditions are to be fulfilled on the wall. On the meniscus, the boundary conditions are expressed as follows,

$$P-P_v+\sigma\kappa = 2\mu\frac{\partial V_n}{\partial n} \tag{6}$$

$$\mu\left(\frac{\partial V_n}{\partial \tau}+\frac{\partial V_\tau}{\partial n}\right) = \frac{\partial \sigma}{\partial \tau} \tag{7}$$

$$V_n = \frac{1}{r}\,(T-T_0) \tag{8}$$

$$-K\frac{\partial T}{\partial n} = h\,(T-T_0)+LV_n\rho \tag{9}$$

Eq. (6) and Eq. (7) express force balance of normal and tangential forces. In Eq. (7), the right hand term is the tangential gradient of the surface tension due to temperature dependence and is written as $\left(\frac{\partial \sigma}{\partial T}\right)\frac{\partial T}{\partial \tau}$. The $\left(\frac{\partial \sigma}{\partial T}\right)$ is a negative constant. In Eq. (8) concept of the evaporation resistance is applied, it means that evaporation velocity on the meniscus is proportion to the temperature jump across the phase boundary. Eq. (9) expresses the heat transfer on the meniscus, the first term of the right handside is the convection heat transfer, the second term is latent heat due to evaporation.

An attempt to solve the Eqs. (3)–(9) was not successful, due to difficulty to

converge numerical solution of Eqs. (3), (4). The first reason is that the finite difference terms of the normal or tangential gradients on the curvilinear boundary in Eqs. (6), (7) have low accuracy. The second one is that the boundary conditions (6)–(9) are implicit. To overcome these difficulties, vorticity and stream-function formulation is applied, by which, explicit boundary conditions can be obtained from Eqs. (7), (8). The vorticity transport equation and Laplace's equation for the stream-function in the (x, y) coordinate system are expressed in the following nondimensional form.

$$\frac{\partial \omega}{\partial t}+U\frac{\partial \omega}{\partial x}+V\frac{\partial \omega}{\partial y}=\frac{\partial^2 \omega}{\partial x^2}+\frac{\partial^2 \omega}{\partial y^2}+Ra\frac{\partial T}{\partial x} \tag{10}$$

$$\frac{\partial^2 \psi}{\partial x^2}+\frac{\partial^2 \psi}{\partial y^2}=-\omega \tag{11}$$

where the vorticity ω and the stream-function ψ are defined as, respectively,

$$\omega=\frac{\partial V}{\partial x}-\frac{\partial U}{\partial y} \tag{12}$$

$$\frac{\partial \psi}{\partial y}=U,\quad \frac{\partial \psi}{\partial x}=-V \tag{13}$$

The boundary conditions on the meniscus of the vorticity and the stream-function are derived from Eqs (7)–(9). The pressure boundary condition is Eq. (6), used only for pressure calculation. Therefore, their nondimensionalized form are expressed as follows.

$$\frac{\partial V_n}{\partial \tau}+\frac{\partial V_\tau}{\partial n}=-Ma\frac{\partial T}{\partial \tau} \tag{14}$$

$$V_n=\frac{1}{R}T \tag{15}$$

$$\frac{\partial T}{\partial n}+(Bic+Bie)\cdot T=0 \quad \text{or} \quad \frac{\partial T}{\partial n}+Bi\cdot T=0$$

where $Ma=\dfrac{|\frac{\partial \sigma}{\partial T}|(T_1-T_0)D}{\mu k}$, $R=\dfrac{\rho L \nu}{D(T_1-T_0)}Pr$,

$$Bi=Bic+Bie,\quad Bic=\frac{Dh}{K},\quad Bie=\frac{D}{Kr}$$

After taking the tangential gradient of Eq. (14), one has

$$\frac{\partial V_n}{\partial \tau}=\frac{1}{R}\frac{\partial T}{\partial \tau} \tag{17}$$

According to definition of the vorticity, the explicit boundary condition for the vorticity is written from Eqs. (15), (17)

$$\omega = \frac{\partial V_n}{\partial \tau} - \frac{\partial V_\tau}{\partial n} = 2\,\frac{\partial V_n}{\partial \tau} - \left(\frac{\partial V_n}{\partial \tau} + \frac{\partial V_\tau}{\partial n}\right) = \left(\frac{2}{R} + Ma\right)\frac{\partial T}{\partial \tau} \tag{18}$$

On the other hand, the evaporating mass rate from the meniscus is,

$$\dot{m} = \rho \Delta_\tau \psi_{i,1} = \rho V_n ds \tag{19}$$

Then considering Eq. (14), the boundary condition for the stream-function is obtained as follows.

$$\Delta_\tau \psi_{i,1} = V_n ds = \frac{T}{R}\, ds$$

or

$$\psi_{i+1,1} - \psi_{i,1} = \frac{T}{R}\, ds \tag{20}$$

Starting from the given value of ψ_0 on the wall, each value of ψ_i on the meniscus is successively calculated.

When the evaporation resistance has a finite value, the exaporating mass is supplied from the bottom of the groove. We assume that the flow there is uniform. Value of this uniform velocity must be determined in such way to satisfy the mass balance for evaporation.

In the following numerical analysis, the necessary equations are Eq. (10), Eq (11), Eq (5) with the boundary conditions Eq. (16), Eq (18), Eq (20). In this mathematical model, six nondimensional parameters appear, which are the Bond number, the Rayleigh number, the Prandtl number, the Biot number, the nondimensional evaporation resistance and the Marangoni number.

3. Numerical Method

3.1 Computation of the meniscus line

The meniscus line equation (2) is a nonlinear ordinary differential equation, and the asymptotic solutions are obtained for the small or large Bond numbers by small perturbation method described in Ref. [1]. Numerical integration is also easily carried out. In our analysis, Eq. (2) is linearized and TDMA (tridiagonal-matrix algorithm) is applied.

$$\frac{d^2 y_0}{dx^2} - Bo\ [1+(\frac{dy_0}{dx})^2]^{3/2} y_0 = 0$$

$$\Delta_{xx} y_0^{m+1} - Bo\ [1+(\Delta_x y_0^m)^2]^{3/2} y_0^{m+1} = 0 \tag{21}$$

the meniscus at the Bond numbers of 1.0 and 100 with the contact angle of 15° are

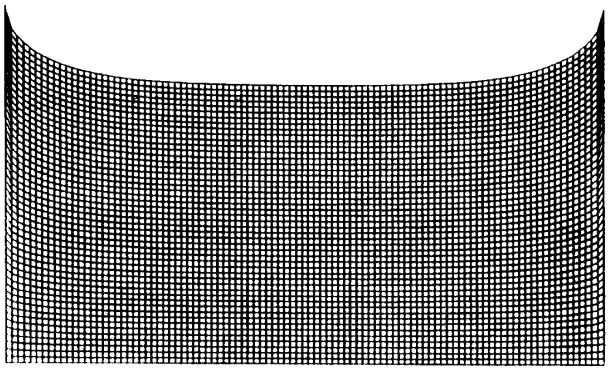

(a)

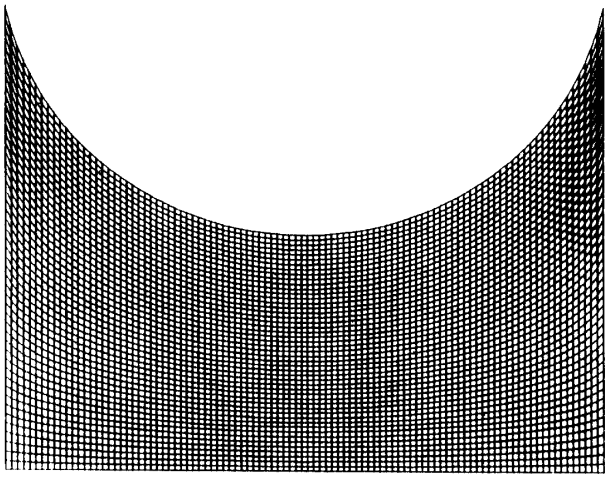

(b)

Fig. 2. Grid system and meniscus, (a) Bo=100, (b) Bo=1.0.

shown in Fig. 2. When liquid is water, a Bond number 1.0 means that the groove width is about 1.0 mm at 1-g environment, or the groove width is about 10 cm in space environment of 10^{-6}g. a Bond number 100 means that the groove width is about 1 cm at 1-g environment, or it is about 1 m in space environment of 10^{-6}g.

3.2 Grid generation and coordinate transformation

A general coordinate system (ξ, η) is introduced in order to make the meniscus coincide with the coordinate surface. The grid system is generated in the physical coordinate (x, y) by algebraic method. Transformation between the physical coordinate (x, y) and the computation coordinate (ξ, η) follows the formula,

$$\begin{aligned} x &= \xi \\ y &= \eta\, y_0\ (x) \end{aligned} \tag{22}$$

The grid system generated by this formula is shown in Fig. 2.

Derivatives of function f(x, y) in the physical coordinate can be expressed by those in the computational coordinate as follows, the first order derivatives are

$$\begin{aligned} f_x &= (y_\eta f_\xi - y_\xi f_n)/J \\ f_y &= (x_\xi f_\eta - x_\eta f_\xi)/J \end{aligned} \tag{23}$$

The second order derivatives appear in the form of Laplacian, which is expressed in the following form,

$$\nabla^2 f = (\alpha f_{\xi\xi} - 2\beta f_{\xi\eta} + \gamma f_{\eta\eta} + \delta f_\eta + \varepsilon f_\xi)/J^2 \tag{24}$$

the normal and tangential derivatives are,

$$\begin{aligned} \frac{\partial f}{\partial n} &= (\gamma f_\eta - \beta f_\xi)/J\sqrt{\gamma} \\ \frac{\partial f}{\partial \tau} &= f_\xi/\sqrt{\gamma} \end{aligned} \tag{25}$$

Where

$$\begin{aligned} J &= x_\xi y_\eta - x_\eta y_\xi \\ \alpha &= x_\eta^2 + y_\eta^2, \quad \beta = x_\xi x_\eta + y_\xi y_\eta, \quad \gamma = x_\xi^2 + x_\eta^2 \\ \delta &= [y_\xi(\alpha x_{\xi\xi} - 2\beta x_{\xi\eta} + \gamma x_{\eta\eta}) - x_\xi(\alpha y_{\xi\xi} - 2\beta y_{\xi\eta} + \gamma y_{\eta\eta})]/J \\ \varepsilon &= [x_\eta(\alpha y_{\xi\xi} - 2\beta y_{\xi\eta} + \gamma y_{\eta\eta}) - y_\eta(\alpha x_{\xi\xi} - 2\beta x_{\xi\eta} + \gamma x_{\eta\eta})]/J \end{aligned}$$

then the governing equations and the boundary conditions for this computation are transformed into the computational coordinate by substituting Eqs. (23)–(25) into Eqs. (5), (10), (11), (16), (18), (20),

$$T_t + U\left(\frac{y_\eta T_\xi - y_\xi T_\eta}{J}\right) + V\left(\frac{x_\xi T_\eta - x_\eta T_\xi}{J}\right) = \frac{1}{P_r}\nabla^2 T \tag{26}$$

$$(\beta T_\eta - \beta T_\xi)/J\sqrt{\gamma} + BiT = 0, \quad \text{on the meniscus} \tag{27}$$

$$\nabla^2 \psi = -\omega \tag{28}$$

$$\Delta_\tau \psi = \frac{T}{R}\, ds, \qquad \text{on the meniscus} \tag{29}$$

$$\omega_t + U\left(\frac{y_\eta \omega_\xi - y_\xi \omega_\eta}{J}\right) + V\left(\frac{x_\xi \omega_\eta - x_\eta \omega_\xi}{J}\right) = \nabla^2 \omega + Ra\,\frac{y_\eta T_\xi - y_\xi T_\eta}{J} \tag{30}$$

$$\omega = \left(\frac{2}{R} + Ma\right) T_\eta/\sqrt{\gamma}, \qquad \text{on the meniscus} \tag{31}$$

3. Computational scheme

Finite difference algorithm is applied to approximate the derivative terms in Eqs. (26)–(31). the implicit time difference scheme is used and these equations are solved by Gauss-Sidel iterative method at each time step. The successive steps in this computation are as follows,

Step 1. $T^n_{m+1}=f_1\ (T^{n-1},\ T^n_m,\ \psi^{n-1})$

step 2. $\psi^n_{m+1}=f_2\ (T^n,\ \psi^n_m,\ \omega^n)$

step 3. $\omega^{n+1}_{m+1}=f_2\ (T^n,\ \psi^n,\ \omega^n,\ \omega^{n+1}_m)$

After a proper initial condition is chosen, the temperature at time step n is calculated at step 1 from Eqs (26)–(27). At the step 2, the stream function at time step n is calculated from Eqs. (28)–(29). At the step 3, the vorticity at time step n+1 is calculated from Eqs. (30)–(31). At each step, iterative process is performed. The index m denotes the number of iterative steps. Then, returning to the step 1, the temperature, the stream function and the vorticity at next step are calculated.

Steady numerical solution is considered to be obtained when the condition

$$\text{Max}\left\{\frac{(T^{n+1}-T^n)}{\frac{1}{2}(T^{n+1}+T^n)}\right\}<10^{-6}$$ is achieved.

4. Numerical Results and Discussions

The flows with the Bond number of 1.0 and the contact angle of 15° were computed by this method. Nondimensional parameters such as the Biot number, or the evaporation resistance can only be determined by experiments, but these data are not readily available. In our analysis, these parameters of different order were used so as to investigate their effects.

At first, the temperature distributions at various condition of the thermal conduction and the thermocapillary convection are compared. When the evaporation resistance is infinite, only the convection effect exists. Further, if both of the Marangoni number and the Rayleigh number are zero, no flow is induced and heat is transferred only by conduction. In Fig. 3, isothermal lines are shown, difference between each line is 0.055 and the maximum temperature is 0.9625. We can see that when the thermocapillary force is acting, the fluid temperature near the side wall is higher than in the case of heat conduction only and the one near the groove center is lower. This means that the thermocapillary force causes convection that the direction of the convection heat transfer is counter to the conduction one near the center, and their directions are same in the region near the side wall. Temperature distributions along the meniscus for the same cases are shown in Fig. 4. This is typical character and as long as the thermocapillary force presents, this type of temperature variation appears.

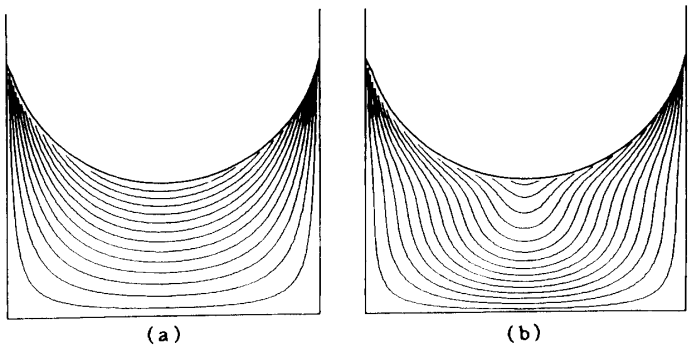

Fig. 3. Temperature field for the heat conduction and the thermocapillary convection, (a) heat conduction, Bi=10, (b) thermocapillary convection, Bi=10, Ma=500.

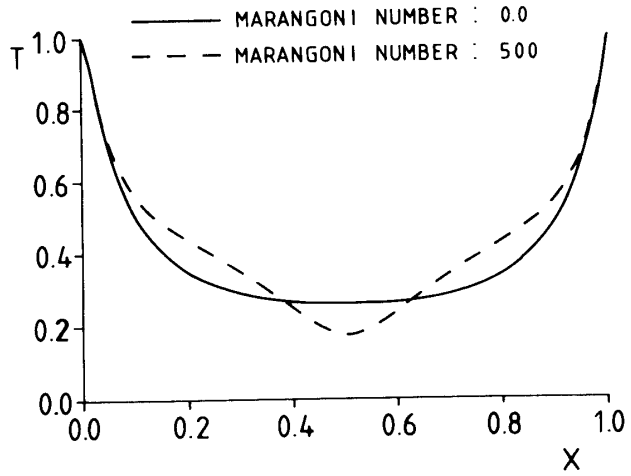

Fig. 4. Temperature distribution along the meniscus, (a) heat conduction, (b) thermocapillary convection.

The thermocapillary flow patterns are compared with buoyancy-driven convection in Fig. 5 and Fig. 6. The flow concentrates in the region near the meniscus in thermocapillary convection, but the buoyancy-driven convection appears in all over the groove.

The numerical results of the evaporating flows are presented in Fig. 7-Fig. 11. Thermocapillary effects are investigated for various evaporation resistance. At the case of a low evaporation resistance R=0.04, shown in Fig. 7, flow pattern scarcely shows any dependence on the Marangoni number. The evaporating flow is dominant and the thermocapillary effect is small. The region near contact line has higher evaporating velocity due to its higher temperature. Therefore, the streamlines curve toward the contact line. When R is increased to 0.2, some change is observed near the meniscus line, as seen in Fig. 8 (b). When R is further increased to 1.0, thermocapillary effect becomes strong, as shown in Fig. 9 (b). Because thermocapillary force drives fluid near the meniscus apart from the contact line, the streamlines adjoining to the meniscus leave apart from the contact line. Therefore, there is counter effects on the meniscus between the evaporation and thermocapillary effect,

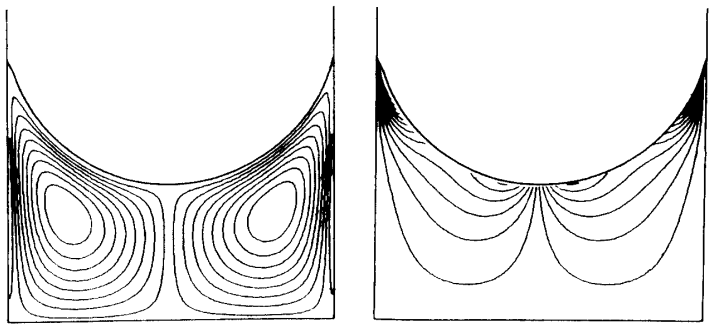

Fig. 5. vorticity for the buoyancy-driven convection and the thermocapillary convection. (a) buoyancy-driven flow, (b) thermocapillary flow.

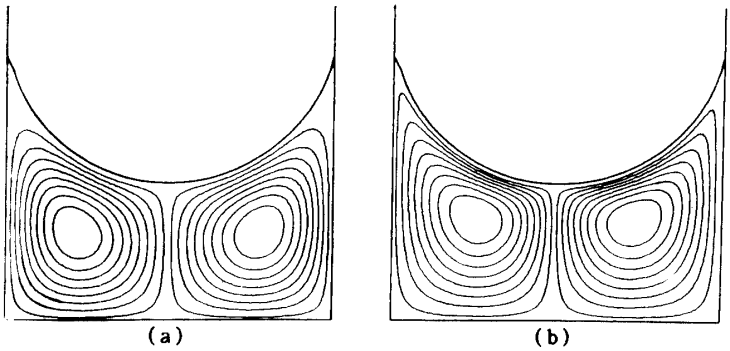

Fig. 6. Streamlines for the buoyancy-driven convection and the thermocapillary convection. (a) buoyancy-driven flow, (b) thermocapillaru flow.

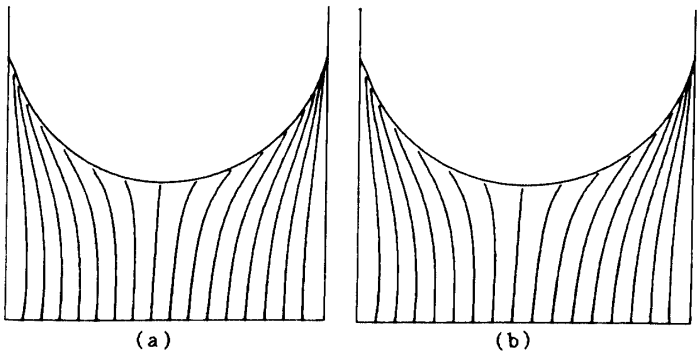

Fig. 7. Streamlines at R=0.04, Bi=30.0. (a) Ma=0, (b) Ma=100.

and this inevitably affects on heat transfer taking place on the meniscus. The thermocapillary effect for the same evaporation resistance value is also shown in Fig. 11. When the Marangoni number increases, a pair of vortices appears and occupies all over the groove as shown in Fig. 11 (a) to Fig. 11 (c).

The temperature distributions on the meniscus with the different Bi are shown in Fig. 10. It is noted that the evaporation resistance R and the evaporation Biot number

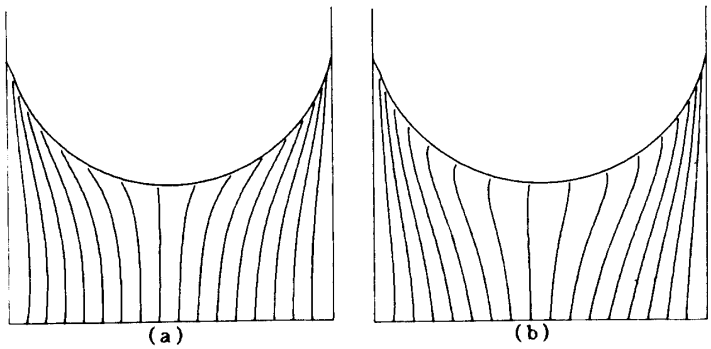

Fig. 8. Streamlines at R=0.2, Bi=10.0. (a) Ma=0, (b) Ma=100.

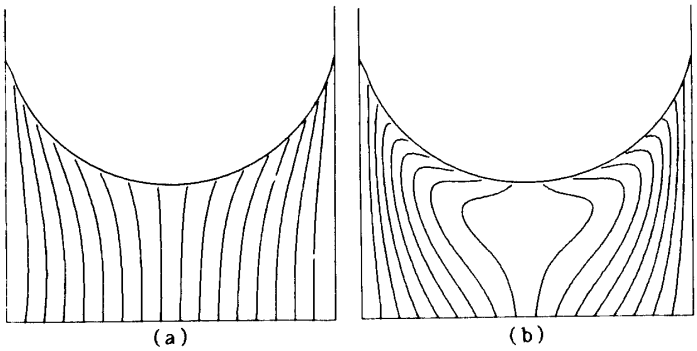

Fig. 9. Streamlines at R=1.0, Bi=2.0. (a) Ma=0, (b) Ma=100.

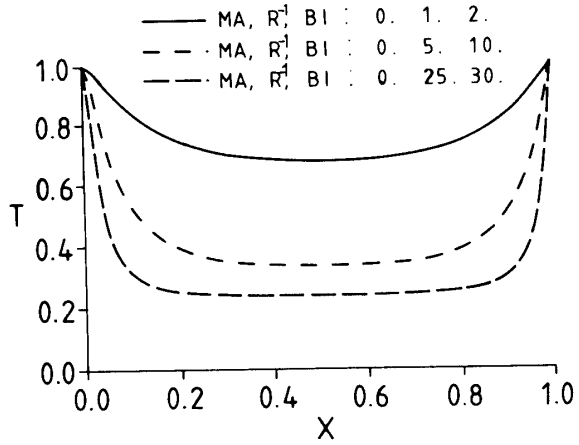

Fig. 10. Temperature distribution along meniscus at various evaporation resistance.

Bie are different only due to the used boundary conditions in the temperature and the stream function. In the evaporating flow, the value of Bic is usually far smaller than Bie. Therefore, Bi≒Bie. Only one out of the Biot number Bi and the evaporation resistance R are independent parameter. usually temperature distributions on the meniscus are mainly determined by R (or Bi). At the smaller evaporation resistance,

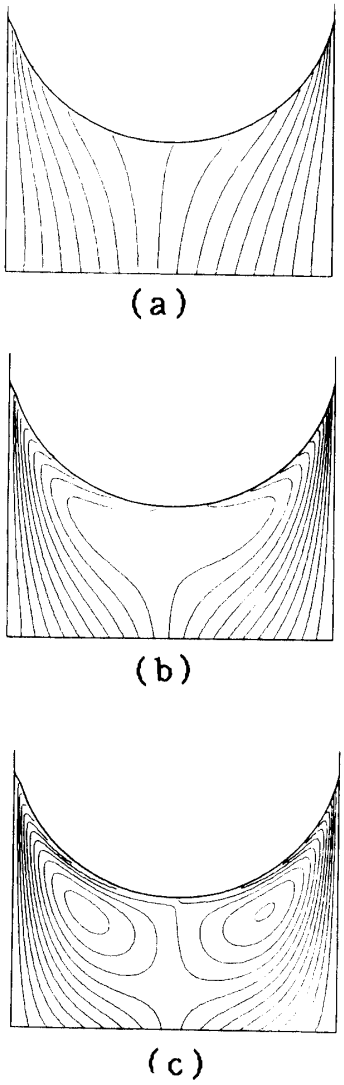

Fig. 11. Streamlines of the flow with various marangoni numbers at R=1, Bi=30, (a) Ma=10, (b) Ma=50, (c) Ma=100.

the temperature is lower as shown in Fig. 10. This may be explained that more heat escapes from the meniscus at a lower evaporation resistance.

On the other hand, heat transfer on meniscus depends upon the temperature distribution along the meniscus and R (or Bi). Here we define $\int_{y_0} Bi \cdot T \cdot ds$ as the capacity of heat transfer, the ds is a small arclength on the meniscus. This quantity at the various Biot and Marangoni numbers is calculated and shown in Tab. 1. At different Marangoni numbers, the change of this quantity is small, not exceeding 5%. They increase when the Biot number increase, but this variation is nonlinear.

Considering that temperature on the meniscus strongly depends upon R (or Bi), it can be said that heat transfer on the meniscus mainly dependent upon R (or Bi). The effect of thermocapillarity did not exceed 5% in the above results. But it is noted that the Biot number (or the evaporation resistance) is assumed to be constant in all

Table 1. Heat transfer rate on the meniscus

Biot number	Marangoni number	Heat transfer
2.0	0.0	0.3854
	500	0.3906
10.0	0.0	1.2062
	500	1.2252
30.0	0.0	2.2083
	500	2.1581

analysis and do not receive any effect of thermocapillarity. However, it is possible that thermocapillarity changes evaporation resistance, because it changes flow pattern on the meniscus, then more effects for heat transfer are brought by thermocapillarity. Relations between thermocapillarity and the evaporation resistance can be determined only by experiments.

5. Conclusion

A two-dimensional mathematical model has been proposed to analyze thermocapillary and evaporating flow. In this model, the concept of evaporation resistance is introduced, by which the explicit boundary conditions can be introduced.

A numerical method using a general coordinate system and grid generation technique has been developed. This method is successful in solving the flow problems in which thermocapillary force acts on the curvilinear meniscus.

Flow problems analyzed in this work are at the low Bond number, the constant Prandtl number, the low or zero Rayleigh number. The effects of the Marangoni number and the evaporation resistance have been investigated, and the heat transfer rate on the meniscus has been numerically predicted. The evaporation resistance is one of the most decisive factor to the heat transfer. Thermocapillary force gives a large effect on the meniscus temperature distribution. However, its effect to the heat transfer rate is not so large.

Experimental data of the thermocapillary effect and the evaporation resistance are lacking.

Only two of six parameters have been investigated in this report. Future numerical work is to investigate effects of the other nondimensional parameters and to analyze unsteady flow problems.

References

[1] P. Concus: Static Menisci in a Vertical Right Circular Cylinder, J. Fluid Mech. (1968), Vol. 34, part 3, pp. 481–495.
[2] S. H. Davis: Thermocapillary Instabilities, Ann. Rev. Fluid Mech. 1987. Vol. 19. pp. 403–435.
[3] P. R. Eiseman: Grid Generation for Fluid Mechanics Computations, Ann. Rev. Fluid Mech. 1985. Vol. 17. pp. 487–522.
[4] L. D. Landau, E. M. Lifshitz: Fluid Mechanics, Pergammon Press Ltd. 1959.
[5] V. G. Levich, V. S. Krylov: Surface-Tension-Driven Phenomena, Ann. Rev. Fluid Mech. 1969. Vol. 1. pp. 293–316.
[6] A. D. Myshkis, V. G. Babaskii, N. D. Kopachevskii, L. A. Sloboshanin, A. D. Tyuptsov: Low-Gravity Fluid mechanics, Springer-Verlag (1987).
[7] S. Ostrach: Low-gravity fluid flows, Ann. Rev Fluid Mech. 1982. Vol. 14. pp. 313–345.
[8] R. Peyret, T. D. Taylor: Computational Method for Fluid Flow, springer-Verlag (1985).
[9] Y. S. Ryazantsev: Thermocapillary Flow of Liquid with Nonlinear Surface Tension Dependence on Temperature. private communication
[10] J. F. Thompson, F. C. Thames, C. W. Mastin: Boundary-Fitted Curvilinear Coordinate System for Solution of Partial Differential Equations on Fields Containing Any Number of Arbitary Two-Dimensional Bodies, NASA CR-2729. (1977).
[11] H. Uchida, K. Kuwahara, S. Enya: Numerical Analysis of Marangoni Convection in Bridgman Method, ISAS Report. SP. 5 (1986). pp. 107–116.
[12] V. A. Wehrle, G. Voulelikas: Evaporation from a Two-Dimensional Meniscus, AIAA J. 1985. Vol. 23. No. 2. pp. 309–313.